Journal of Industrial and Engineering Chemistry 149 (2025) 355–365

Contents lists available at ScienceDirect

Journal of Industrial and Engineering Chemistry

journal homepage: www.elsevier.com/locate/jiec

Advanced dual-wetting membrane for enhanced CO_2 capture: Asymmetric hydrophobic and CO_2-philic thin film in membrane gas absorption

Pei Thing Chang [a], Qi Hwa Ng [b], Pei Ching Oh [c], Siew Chun Low [a,*]

[a] School of Chemical Engineering, Universiti Sains Malaysia 14300 Nibong Tebal, Penang, Malaysia
[b] Faculty of Chemical Engineering & Technology, Universiti Malaysia Perlis 02600 Arau, Perlis, Malaysia
[c] CO_2 Research Centre (CO2RES), Chemical Engineering Department, Universiti Teknologi PETRONAS, 32610 Tronoh, Perak, Malaysia

ARTICLE INFO

Keywords:
Asymmetric wetting
CO_2 capture
Graphene oxide
Membrane Gas Absorption
Superhydrophobic

ABSTRACT

CO_2 is a major contributor to climate change, making efficient carbon capture essential for emission reduction. Membrane gas absorption (MGA) offers a cost-effective solution, with research often focusing on enhancing membrane hydrophobicity to reduce wettability. However, the potential of CO_2-philic membranes for mixed gas separation remains underexplored. This study addresses the gap by developing asymmetric wetting membranes (PVDF/EDA/GO) with a superhydrophobic side to prevent wetting and a CO_2-philic side to enhance CO_2 capture. The CO_2-philic surface was created by coating PVDF with ethylenediamine (EDA) and graphene oxide (GO). Computational analysis confirmed strong binding energy (−21.07 kcal/mol) between EDA and GO, forming a stable amine complex. The membranes displayed asymmetric wetting, with the CO_2-philic side showing a water static angle (WSA) of 49.6 ± 2.6°, and the superhydrophobic side achieved a WSA of 149.7 ± 3.3° and a water gliding angle (WGA) of 9.8 ± 1.1°. In MGA, these membranes demonstrated improved performance, with a CO_2 absorption flux of 0.0040 mol/m^{2}s and CO_2/N_2 selectivity of 6. This work highlights the promise of dual-wetting membranes for enhancing CO_2 capture in MGA systems.

Introduction

The increasing severity of climate issues has made carbon dioxide emissions a major global concern. To address this, post-combustion CO_2 capture has been identified as an effective strategy for reducing CO_2 emission specifically from fossil fuel power plants. Recently, membrane gas absorption (MGA) technology has received widespread interest because of its operational versatility and great energy efficiency in capturing CO_2 [1,2]. It is an absorption process in which a microporous and hydrophobic membrane is utilized to provide a non-mixing boundary between the liquid absorbent and gas flow [3]. In contrast to conventional amine absorption technologies, such as packed-column systems, MGA offers large interface area, small equipment size and allows separate regulation of gas and liquid flow velocities, which helps to overcome the typical operational challenges encountered by packed towers, such as flooding, channeling, foaming and entrainment [4].

After years of MGA research and development, great progress has been made in CO_2 emission reduction. Specifically, the enhancement of membrane hydrophobicity greatly improves CO_2 absorption [5]. Jin et al. [6] found that membrane with enhanced hydrophobicity exhibited more stable and higher CO_2 absorption flux during 300 mins of MGA operation. In another attempt by Rosli et al. [7], they enhanced the hydrophobicity of PVDF membrane, resulting in long-term CO_2 absorption stability. Despite 120 days of exposure to the corrosive amine absorbent, the membrane maintained a constant flux. Since membrane hydrophobicity is an important indicator for MGA performance, researchers have proposed different strategies to fabricate superhydrophobic membranes to prevent membrane wetting. Teoh et al. [8] proposed a template printing strategy to print multiscale micro- and nanostructures on the membrane surface by casting polymer dope on nonwoven substrate. These hierarchical structures promote air entrapment between the liquid and the membrane, maintaining a stable Cassie-Baxter state for the gas–solid-liquid (air-membrane-water) interface. By displaying a WSA of 156° and a GWA of 5°, the templated polymer matrix exhibits excellent wetting resistance. In a different study by Zhao et al. [9], the same template printing method was employed using stainless-steel mesh and successfully produced an excellent water repellent PVDF membrane. The developed membrane recorded a WSA and water GWA of 164° and 6.8° respectively.

Although the membrane's hydrophobicity has been enhanced, it

* Corresponding author.
E-mail address: chsclow@usm.my (S.C. Low).

https://doi.org/10.1016/j.jiec.2025.01.047
Received 28 October 2024; Received in revised form 30 December 2024; Accepted 26 January 2025
Available online 6 February 2025

does not improve CO_2 diffusion across the membrane to better absorption by the amine absorbent. Lin et al. [10] discovered that increasing the membrane hydrophobicity from 100° to 125° managed to maintain the CO_2 capture in membrane contactor for 21 days. However, the CO_2 absorption flux was found to be not as high as that of the pristine PVDF membrane and was relatively low. This is because the deposition of modified layer on the PVDF membrane surface, inducing a hydrophobic delayed wetting function but does not provide an affinity attraction to CO_2. Therefore, the CO_2 attraction is only relied on the liquid absorbent, which will result in lower CO_2 absorption flux. Following this line of thought, developing a membrane with asymmetric surface wettability, with a CO_2-philic surface on one side and a superhydrophobic surface on the other, could be an effective strategy to simultaneously reduce membrane wetting and enhance CO_2 passage through the membrane [11].

Asymmetric surface wetting membrane, also known as Janus membrane, is usually defined as membrane having contrasting wetting characteristic on both sides, namely hydrophobicity and hydrophilicity. It has been widely reported in membrane distillation (MD) that the hydrophilic surface repels fouling components, while the hydrophobic surface alleviates wetting. Chen et al. [12] constructed a hydrophilic top layer of polydopamine and polyethyleneimine on a hydrophobic PVDF membrane. Their Janus membranes showed increased flux, delayed membrane wetting and resistance to oil fouling during MD. Inspired by the Janus membrane concept in MD, a "double-sided" membrane with asymmetric surface wettability, i.e., a CO_2-philic surface and a superhydrophobic surface, is likely to be used for MGA. The CO_2-philic surface faces the gas phase to increase the attractive CO_2 movement towards the membrane, while the superhydrophobic surface on the opposite side faces the liquid phase to assist in hindering wetting. The CO_2-philic surface is usually composed of functional groups with high affinity for CO_2, such as hydroxyl [13], carbonyl, thiocarbonyl, carboxyl, amine [14] and amide groups. Based on this principle, materials composed of these functional groups such as graphene oxide (GO) can be utilized to form a layer that attracts CO_2 on hydrophobic-based membranes.

GO is widely used in membrane design for liquid and gas separation due to its oxygen-containing functional groups including C=O, C-O-C, –OH, and –COOH groups. –OH and –COOH groups are usually found at the edges, while C-O-C are found on the basal plane. These groups confer good hydrophilicity and easy dispersion in water, resulting in stable suspensions through electrostatic repulsion. GO's affinity for CO_2 makes it a popular choice in membrane synthesis for CO_2 separation [15]. GO-based membranes are categorized as mixed-matrix and laminated, with laminated GO membrane offering better CO_2 selectivity [16], due to orderly aligned polar groups on the surface, providing preferential CO_2 interaction sires. These functional groups also maintain interspaces between GO nanosheets to create efficient transport channels [17]. Shen et al. [18], for instance, observed that a two-fold increase in CO_2 permeability with GO incorporation. Consequently, GO membranes significantly enhance CO_2 selectivity.

To the best of our knowledge, asymmetric wetting membranes with robust anti-wetting surface and CO_2-philic surface have not been reported in MGA applications. Therefore, the main contribution of this work is to design an asymmetric wetting membrane for MGA to simultaneously overcome the wetting and low flux issues. Based on our previous work [19], superhydrophobic surface can be generated by surface template printing to create hierarchically rough surface. In this work, the other side of the membrane is designed with a thin layer of CO_2-philic GO and EDA as cross-linker through a simple surface coating method. The CO_2 uptake performance of these asymmetric wetting membranes in MGA is studied using AMP as a liquid absorbent. AMP is chosen because it has a high capacity for CO_2 absorption, good thermal stability and lower regeneration energy [20]. The underlying mechanism for enhancing the attractiveness of the membrane to CO_2 is elucidated by analyzing the membrane' structural and chemical attributes.

Methodology

Fabrication of asymmetric wetting membrane

Flat sheet PVDF membranes with asymmetric wetting (Fig. 1) were produced in two stages. First, a superhydrophobic surface was created using template printing with a nonwoven substrate [21]. Then, the other side of the membrane was modified to generate a CO_2-philic surface. Briefly, PVDF dope was prepared by dissolving PVDF powder (Alfa Aesar, United State), previously dried at 90 °C in an oven, into a 60 °C heated NMP (Sigma Aldrich, Germany) solution (15/85 wt ratio). The dope was degassed and cast onto a 400-um thick nonwoven substrate and submerged in a water precipitation bath for one day to solidify. The membrane underwent air-drying continuously for 3 days and then carefully separated from the substrate, replicating the nonwoven structure on its surface.

The membrane fabrication process was then continued with the modification of the underside, which corresponded to the non-patterned side of the superhydrophobic surface. For the PVDF/EDA/GO composite membrane, the non-patterned side was first treated with a 5 M EDA (Sigma Aldrich, Germany) solution at 80 °C for 1 h and subsequently air-dried. Following this step, the surface was coated with a 0.25 mg/mL GO solution (lateral size:1–5 um, thickness: 0.8–1.2 nm and single layer ratio: >99 % from Jcnano, China) at room temperature (25 °C) for 30 min, followed by air-drying. Before the coating process, the GO solution (0.25 mg/mL) was subjected to sonication for 30 min to ensure uniform dispersion. The GO coating process was repeated 5 times. The unmodified membrane is referred to as the pristine PVDF membrane, while the membrane modified to achieve asymmetric wetting characteristics is designated as the PVDF/EDA/GO composite membrane.

Membrane characterizations

The superhydrophobic aspect of the membrane has been detailed in previous studies [19]. This work focuses on creating a CO_2-philic surface for asymmetric wetting. Membrane characterizations emphasized the CO_2-philic properties, analyzed using scanning electron microscope (SEM) to determine the surface morphology, porosity and pores distribution via ImageJ software. Surface porosity was calculated by constructing a 3D surface map from SEM images and using the "threshold" tool in ImageJ to determine the perforated area ratio. Around 100 membrane pores were manually examined based on the SEM surface topography, and pore size distribution was categorized using OriginPro

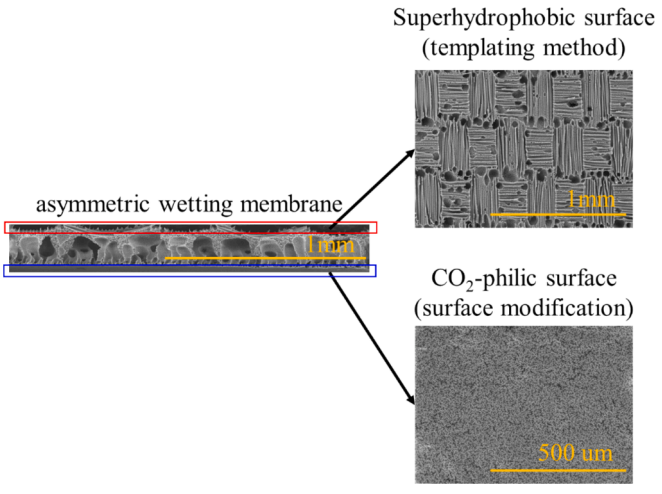

Fig. 1. SEM images of asymmetric wetting of PVDF membrane.

2018 software. The membranes' functional groups were assessed using ATR-FTIR spectroscopy covering wavenumbers from 4000 cm^{-1} down to 400 cm^{-1}. Atomic elemental analysis for carbon, fluorine, and oxygen was conducted using EDS (FEI, Quanta 450 FEG, Czech Republic). The membrane surface topography was examined using confocal laser scanning microscope (CLSM, Zeiss LSM700 MAT with Axio Imager). Surface wetting characteristics were evaluated by measuring contact angles of stationary water droplet (WSA) and water gliding angle (WGA) using a surface gauge.

The membrane thickness was measured by using micrometer screw gauge. The membrane bulk porosity was determined by immersing membrane sample in 2-butanol for 2 h. After immersion, the wetted membrane was weighed followed by dried in an oven until completely dry. Subsequently, the dried membrane (m_d) was weighed. The bulk porosity (%) was calculated using the following equation:

$$Bulk\ porosity(\%) = \frac{\frac{(m_w - m_d)}{\rho_b}}{\frac{(m_w - m_d)}{\rho_b + \frac{m_d}{\rho_m}}} \times 100\% \quad (1)$$

where the ρ_b and ρ_m are the density of 2-butanol and membrane respectively.

Mixed gas MGA performance

The MGA system operated under atmospheric pressure and room temperature (25 °C), as shown in Fig. 2. The CO_2-philic layer faced the gas phase to increase CO_2 affinity, while the patterned rough surface faced the liquid amine absorbent to prevent membrane wetting (membrane effective surface area of 9.62 cm^2). A CO_2/N_2 gas mixture (20/80 and 30/70 vol ratios) was maintained at 200 mL/min with a mass flow controller. At the same time, the AMP (Merck, Germany) liquid absorbent flowed on the opposite side via a peristaltic pump at 120 mL/min. The gas mixture before and after the MGA process was collected in a 1 L gas bag for GC analysis. CO_2 absorption flux, J (mol/m^2s) and selectivity of CO_2 over N_2 were calculated using Eq. (2) and (3).

$$J\ (mol/m^2s) = \frac{(Q_{g,i} - Q_{g,o})\rho_g}{MW_g A} \quad (2)$$

$$Selectivity = \frac{\frac{y_{CO2}}{y_{N2}\ permeate}}{\frac{y_{CO2}}{y_{N2}\ feed}} \quad (3)$$

where feed ($Q_{g,i}$) and retentate ($Q_{g,o}$) of CO_2 are set at mL/min, ρ_g (g/mL) and MW_g (g/mol) are the density and molecular weight of targeted CO_2 gas respectively, A refers to the membrane's area in m^2, and y_{CO2} and y_{N2} are the concentrations of CO_2 and N_2.

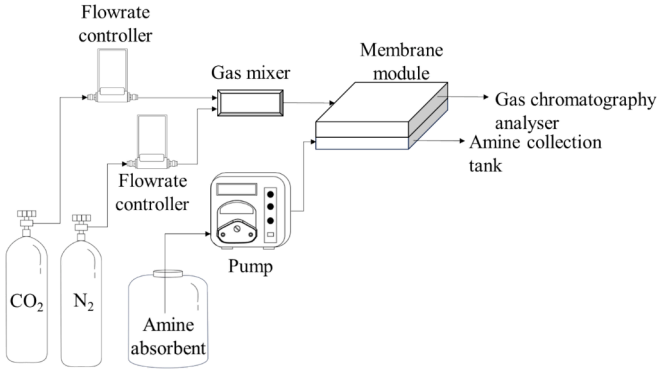

Fig. 2. Schematic diagram of MGA system.

Mass transfer analysis

The complete mass transfer process in MGA involves three stages: the movement of gas from the gas phase to the membrane surface, diffusion through the membrane pores, and the transfer from the membrane surface to the liquid phase. The process is represented by the resistance-in-series model, given by:

$$\frac{1}{K_{ol}} = \frac{1}{k_g} + \frac{1}{k_m} + \frac{1}{Hk_l} \quad (4)$$

where $1/K_{ol}$ represents the resistance of overall mass transfer (s/m), $1/k_g$, $1/k_m$ and $1/Hk_l$ represent the resistances (s/m) of the gas phase boundary layer, the membrane and liquid phase boundary layer, respectively, and H is Henry's constant. K_{ol} can be obtained experimentally using:

$$K_{ol} = \frac{J}{\Delta C_m} \quad (5)$$

where ΔC_m is the logarithmic mean concentration driving force (mol/m^3). In MGA operated under non-wetted mode, the gas phase resistance is negligible:

$$\frac{1}{K_{ol}} = \frac{1}{k_m} + \frac{1}{Hk_l} \quad (6)$$

The membrane mass transfer resistance, $1/k_m$, is depicted as:

$$\frac{1}{k_m} = \frac{\tau\delta}{D_{CO2,m}\,\varepsilon} \quad (7)$$

In this context, D_{CO2} represents the apparent diffusion coefficient of CO_2 across the membrane (m^2/s), ε denotes the MGA's porosity, δ indicates the membrane's thickness (m) and τ refers to the membrane's tortuosity, estimated by:

$$\tau = \frac{(2-\varepsilon)^2}{\varepsilon} \quad (8)$$

CO_2 diffusion through the membrane is governed by Knudsen diffusion:

$$\frac{1}{D_{co2,m}} = \frac{1}{D_{Kn}} \quad (9)$$

The Knudsen diffusion coefficient, D_{kn} (m^2/s) is calculated by:

$$D_{Kn} = \frac{d}{3}\sqrt{\frac{8RT}{\pi M_{CO2}}} \quad (10)$$

where d is the mean membrane pore diameter (m) and M_{CO2} is the molecular weight of CO_2 (kg/mol). Using Eq. (7) to (10), the $1/k_m$ can be determined, and consequently, $1/Hk_l$ can be calculated through Eq. (6).

Computational simulations of atomic energy

The analysis of molecular interactions between EDA, GO and PVDF membrane was conducted using HyperChem 8 (Hypercube Inc). Molecular structures of EDA and GO were simulated within a simulation box, employing semi-empirical mechanic (PM3) to determine their lowest energy structure. Geometry optimization was performed using the Polak-Ribiere method, following the NDDO approximation. The Fock matrix elements within this framework are defined as:

$$F_{\mu\nu} = H_{\mu\nu} + \sum_{B(\neq A)} \sum_{\lambda,\sigma}^{B} P_{\lambda,\sigma}(\mu\nu|\lambda\alpha) - \frac{1}{2}\sum_{\lambda,\sigma}^{A} P_{\lambda,\sigma}(\mu\nu|\lambda\sigma) \quad (11)$$

where H is the core Hamiltonian matrix element, P is the valence electron density matrix and $(\mu\nu|\lambda\sigma)$ are the two-center-two-election repulsion integrals. To examine the possible interactions between EDA and

GO, the binding energy, ΔE_N was calculated using:

$$\Delta E_N = \sum E_{complex} - \sum E_{individual\ components} \quad (12)$$

where $E_{complex}$ is the energy of the molecular complex, and $E_{individual\ component}$ is the energy of the individual molecules.

Results and discussion

Mass transfer analysis

Before examining the impact of the CO_2-philic layer on CO_2 capture, it was necessary to identify the dominant mass transfer resistance in the MGA process. Fig. 3a depicts the influence of mixed gas flowrate on CO_2 absorption flux, while holding the AMP absorbent flowrate steady at 120 mL/min. Despite the gas velocity increasing from 100 to 200 mL/min, the CO_2 absorption flux remained stable, ranging between 4.04 and 4.46 $\times$ 10^{-3} mol/m^2s. This observation suggests that variations in feed gas flowrate have a negligible impact on CO_2 absorption flux and overall mass transfer resistance. This stability can be attributed to the adequacy of the AMP absorbent, which effectively absorb CO_2 from the feed gas, thereby maintaining a consistent reaction rate between CO_2 and AMP. To enhance CO_2 flux through the membrane, upgrading the membrane surface with a CO_2-philic layer is expected to improve MGA performance, rather than relying solely on amine absorbent on the other side of the membrane. It is anticipated that membranes with CO_2-philic layers induced by EDA-GO will draw more CO_2 molecules closer membrane's interface, facilitating their passage across the porous polymer matrix and into amine absorbent.

Fig. 3b shows that with an increased in AMP absorbent flowrate from 65 to 130 mL/min, there was a substantial reduction in the CO_2 absorption flux. Specifically, the flux dropped nearly two-fold, from 7.18 $\times$ 10^{-3} to 3.84 $\times$ 10^{-3} mol/m^2s, when the absorbent flowrate was doubled. This trend contrasts with previous studies, such as Hashemifard et al.[22] and Cao et al. [23], which reported increased CO_2 absorption flux with higher absorbent flowrates. The difference can be attributed to reduced contact time between the gas and liquid phases at higher absorbent flowrates, limiting CO_2 dissolution in the AMP absorbent. The dominant factor influencing the CO_2 absorption flux, as depicted in Fig. 3a and 3b, is the flowrate of AMP absorbent, while gas velocity has relatively minor effect. This suggests that the primary mass transfer resistance occurs within the liquid phase.

In the MGA process, gas flowrate is generally considered inconsequential due to the dominance of liquid-side mass transfer resistance, as evidenced in Fig. 3, where CO_2 absorption primarily occurs within the liquid film. Thus, the overall mass transfer resistance ($1/K_{ol}$) for the PVDF membrane remained consistent under similar AMP absorbent flowrate. $1/Hk_l$ was calculated based on $1/K_{ol}$ and membrane mass transfer resistance ($1/k_m$) using Eq. (6). Fig. 4a displays the relationship between the AMP flowrate and the $1/K_{ol}$. A decrease in AMP flowrate resulted in a decrease in $1/K_{ol}$ from 2248.89 to 1221.24 s/m (approximately two-fold lower) as the AMP flowrate decreased from 130 to 65 mL/min. Fig. 4b delineates the contribution of $1/Hk_l$ and $1/k_m$ at different AMP flowrates. It was observed that $1/Hk_l$ consistently contributed a higher resistance compared to $1/k_m$. Specifically, $1/Hk_l$ accounted for approximately 99 % of the overall mass transfer resistance during the separation process at a feed gas flowrate of 200 mL/min. As the AMP flowrate decreased from 130 to 65 mL/min, $1/Hk_l$ decreased

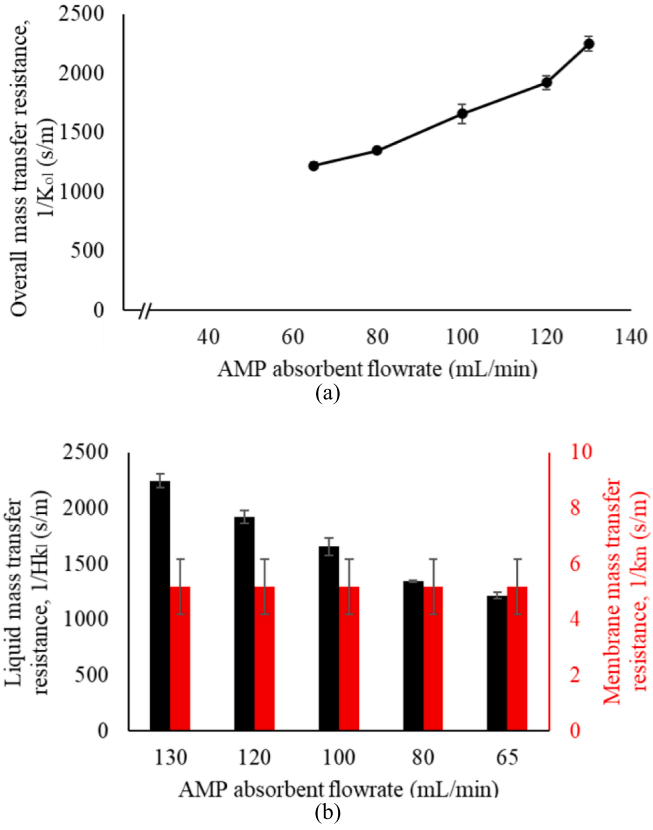

Fig. 4. (a) $1/K_{ol}$ and (b) specific mass transfer resistance based on the absorbent flowrate.

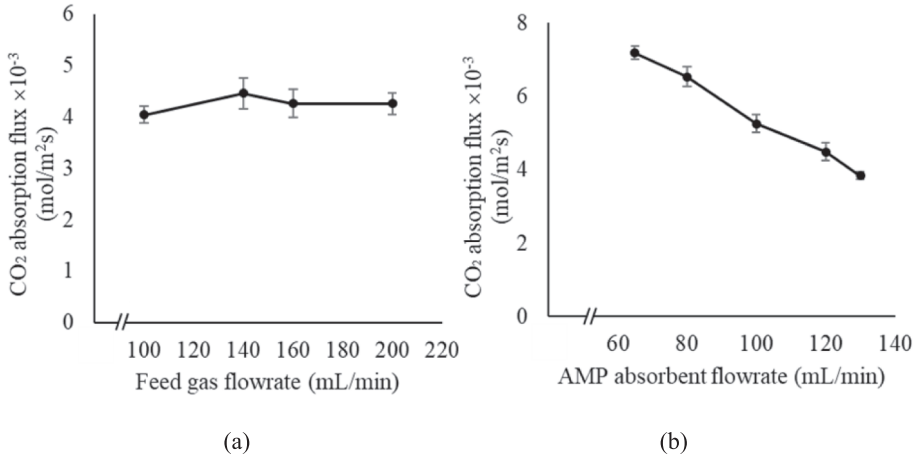

Fig. 3. Effect of (a) feed gas flowrate and (b) absorbent flowrate.

from 2243.71 to 1216.06 s/m. These findings indicate the predominant role of $1/Hk_l$ in CO_2 absorption in the gas–liquid interface system, particularly when using the superhydrophobic membrane. Therefore, optimizing and controlling absorbent flowrate in practical industrial applications is imperative to mitigate mass transfer resistance attributed to the liquid boundary layer, thereby enhancing the mass transfer coefficient of the MGA process.

Evaluation of membrane characteristics

Surface modification of pristine PVDF with EDA and GO induces changes in surface chemistry and hydrophobicity. ATR-FTIR analysis of the surface-coated membranes (Fig. 5a) confirms successful deposition of EDA and GO onto the CO_2-philic layers. Characteristic PVDF peaks at 3020 and 2980 cm^{-1} (C–H stretching and deformation vibrations) and 1170 cm^{-1} (CF_2 stretching) are observed. Notable changes are evident in FTIR spectrum of the PVDF/EDA/GO membrane, reflecting alterations in chemical bonding. Peaks at 3300 to 3600 cm^{-1} represent O–H stretching vibrations from GO hydroxyl group, while peaks at 1735 cm^{-1} and 1650 cm^{-1} correspond to C=O stretching from GO carbonyl groups and N–H bending from EDA primary amines [24,25]. These shifts confirm that EDA and GO have appeared as the uppermost layer of membrane.

The strength of the CO_2-philic coating (GO) on the PVDF membrane is highly dependent on the atomic interactions between PVDF and EDA, to achieve minimum energy of the system. Therefore, simulating their atomic bond interactions is crucial to support the discussion of their organic–inorganic compatibility and defect-free interface. HyperChem was used for this purpose and the calculated bond energies are displayed in Fig. 6. It is widely acknowledged that PVDF has a stable carbon backbone with multiple C-F bonds and is not reactive. The inertness of PVDF makes its backbone chain hardly break. However, PVDF still has the potential to form hydrogen bonds with surrounding molecules. To elucidate the possibility of hydrogen bonding between PVDF and EDA, the molecular interactions of PVDF with EDA were simulated in the periodic box. Geometry-optimized PVDF and EDA structures obtained

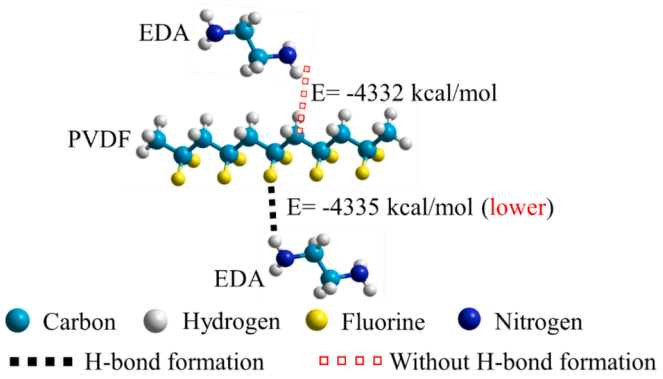

Fig. 6. Energy interaction of PVDF/EDA membranes calculated from HyperChem.

by the PM3 method were allowed to rotate in periodic boxes to inhibit hydrogen bonding, as described by Rosli et al. [26], to produce the composite combinations with the lowest energy. The energy difference between the presence (black dashed lines in Fig. 6) and absence (red dashed lines in Fig. 6) of hydrogen bonds in PVDF/EDA are compared. Overall, the energies of PVDF/EDA with hydrogen bonding (−4335 kcal/mol) are slightly lower compared to those without hydrogen bonding (−4332 kcal/mol). Complexes with low binding energy (the most negative ones) form more steadily. This suggests the existence of atomic interactions between the PVDF polymer and the EDA. This computational finding (Fig. 6) aligns with FTIR result in Fig. 5a, which confirmed the amine group from EDA presence on the surface of PVDF/EDA/GO membrane. The fluorine groups within PVDF have higher probability of forming hydrogen bonds with the amine groups of EDA, substantiating the role of EDA as a stable intermediary that establishes a connection between the polymer substrate and the GO layer. This finding is supported by similar experimental outcomes from Eum et al. [27] and Meng et al. [17], where EDA coatings facilitates strong adherence of GO nanoparticles and improved stability between GO and

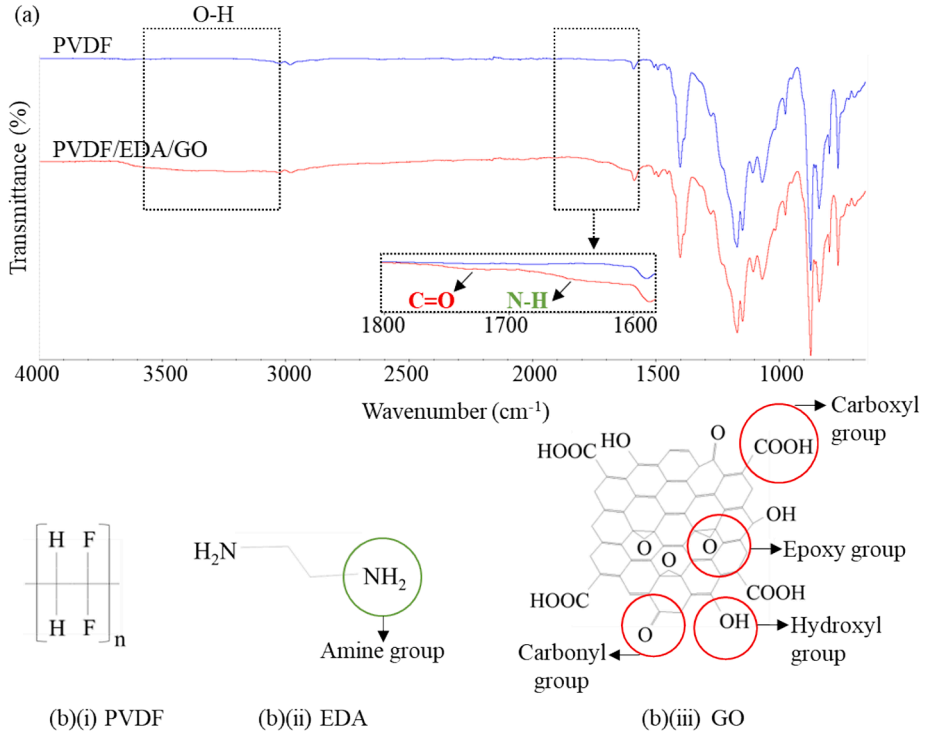

Fig. 5. (a) FTIR spectra of pristine PVDF and PVDF/EDA/GO membranes and (b) structure of (i) PVDF, (ii) EDA and (iii) GO.

the membrane substrate.

The deposition of GO onto the EDA-treated membrane surface results in two possible chemical reactions, which are elucidated in Fig. 7. The first chemical reaction (reaction (1) indicated by the blue line) is an amine group from EDA reacting with a carboxyl group from GO. The binding energy of EDA and GO is + 214.37 kcal/mol according to the simulated atomic interactions. A positive value of binding energy indicates that energy must be supplied to the reaction, in other words, this reaction is unlikely to occur. Whereas for reaction (2) (represented by the red line), the amine groups of EDA interact with the epoxy groups on GO, leading to the formation of secondary amines and hydroxyl groups. By using the similar binding energy calculation, the binding energy of the amine to the epoxide is −21.07 kcal/mol. This means that the epoxy group on GO is likely to react with the amine group of EDA to form a secondary amine, forming a complex where EDA is linked to GO. The aliphatic chain of EDA donates electrons to the amine functional group, making it a strong nucleophile. Then, it promotes the nucleophilic ring opening of epoxy groups on GO, resulting in the formation of hydroxyl groups on GO. This finding, derived from the simulated atomic energy in Fig. 7, correlates with the FTIR spectra shown in Fig. 5, where the asymmetrical aromatic C-O stretch is not clearly detected after modification with GO. In addition, the hydroxyl groups formed during the ring opening process of oxirane ring are beneficial to accelerate the reaction of epoxy-amines. This reaction is also known as autocatalytic behavior. Therefore, reaction (2) (amine reacts with epoxide) is the predominant interaction between EDA and GO.

However, competition arises between GO and PVDF for interaction with amines. The amine groups within EDA engage not only with the epoxy groups in GO (depicted in Fig. 7), but also establish hydrogen bonds with the PVDF base membrane (as shown in Fig. 6). After EDA depositing onto the PVDF membrane, the available amine groups for interaction with epoxy groups (GO) reduces, possibly resulting in a lower degree of epoxy-amine reactivity on the membrane surface. Since the epoxy groups of GO compete with PVDF polymer to interact with the amine bond of EDA, the GO coating solution may diffuse into the EDA layer, resulting in the mixing of the top layer (GO) and the second layer (EDA) [28]. If the GO coating solution intrudes into the EDA layer, this may result in a reduced density of GO on the upper surface, consequently hampering CO_2 absorption. Moreover, the penetration of the GO solution may occupy the porous structure of EDA, causing the composite membrane to form a denser layer, which adversely affects the MGA performance. After the correlating simulation results with experimentally synthesized membranes, SEM images were taken to observe the morphological evolution of both pristine and modified membranes (PVDF and PVDF/EDA/GO), as illustrated in Fig. 8a. The pristine PVDF membrane (Fig. 8a-i) showed a lacy interconnected porous structure. This structure emerges from the rapid exchange of solvent (NMP) and non-solvent (water) during membrane coagulation in the coagulation bath. The high degree of immiscibility between polymers and non-solvents result in this porous and open-pore structures, which proves beneficial for MGA by reducing mass transfer resistance for CO_2 to pass through the membrane [29]. After EDA treatment, the carbon backbone of PVDF forms cross-links with EDA amine. As depicted in Fig. 7, the oxygen-containing functional groups within GO exhibit high reactivity towards EDA amines, resulting in the spontaneous attachment of GO sheets to the membrane surface. This outcome is clearly visible in the SEM image. The GO sheets are randomly dispersed across the membrane, without fully covering its surface. The SEM image presented in Fig. 8a-ii validates that the intrinsic porous structure remains intact even after the deposition of the thin GO layer on the porous PVDF membrane. This is further supported by the bulk porosity measurements, which show that the overall bulk porosity remains at 86.3 ± 0.2 % after the EDA-GO deposition, closely matching that of the pristine PVDF membrane (87.0 ± 0.9 %). Additionally, the membrane thickness of the PVDF/EDA/GO membrane showed no significant increase, measuring at 216 ± 11 um compared to 215 ± 9 um for the pristine PVDF membrane. This confirms that the GO layer formed only as a thin coating. Indeed, maintaining membrane porosity and thickness are vital for MGA application, as a thick CO_2-philic layer on the PVDF membrane surface would increase mass transfer resistance, which reducing CO_2 permeation. These findings demonstrate the successful deposition of GO onto the EDA-treated membrane surface without significantly altering the membrane's porous structure.

While the membranes bulk porosity and thickness remained unaffected, the roughness of the membranes increased slightly. The average surface roughness (R_a) increased from 0.0544 ± 0.0017 um for the pristine PVDF to 0.0624 ± 0.0012 um for the PVDF/EDA/GO membrane, as depicted in Fig. 8c. The slight increase in surface roughness is attributed to the localized accumulation of GO on certain areas of the membrane surface, as observed in Fig. 8-ii. However, the difference in R_a (approximately 0.0080 um or 8 nm) is minimal, indicating that the GO accumulation had a negligible impact on the overall membrane structure.

As shown in Fig. 8b, EDS analysis was used for additional insight into the element compositions of both the pristine PVDF and modified membranes surface. During the EDS analysis, it is expected that carbon (C) and fluorine (F) elements will be detected in both membranes, as these elements are inherent to the PVDF structure. For the pristine

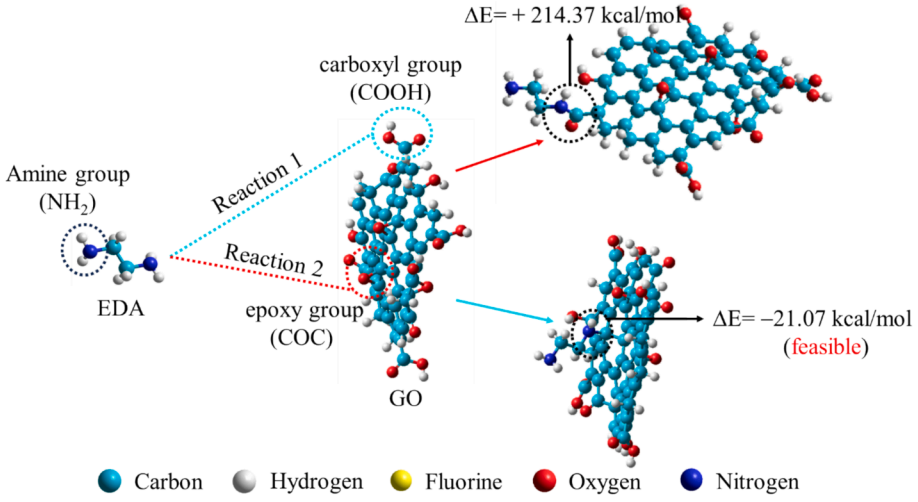

Fig. 7. The binding energies of EDA with GO through (i) Reaction path 1 (blue line): GO (carboxyl group) with EDA (amine group) and (ii) Reaction path 2 (red line): GO (epoxy group) with EDA (amine group). Binding energies were simulated using HyperChem.

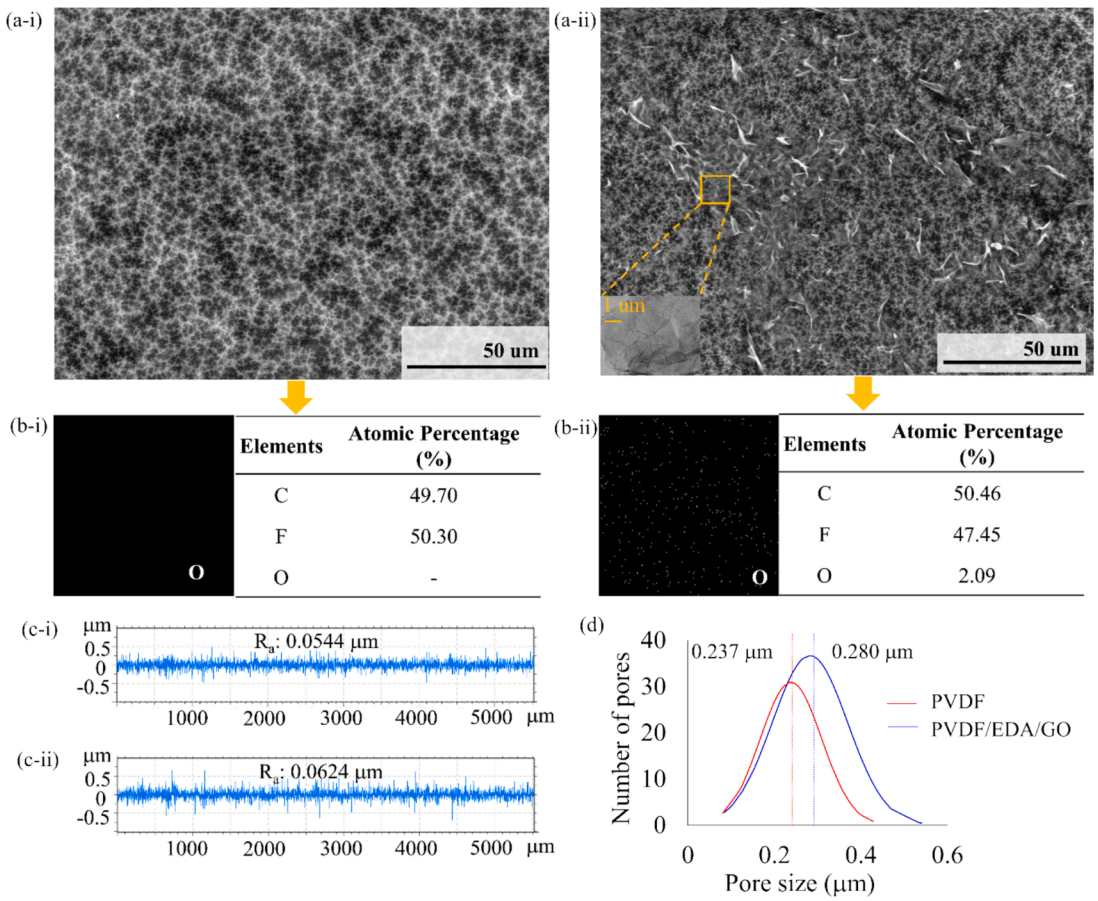

Fig. 8. (a) SEM images, (b) EDS composition and mapping of O element on membrane surface and (c) surface roughness profile of (i) pristine PVDF and (ii) PVDF/EDA/GO membranes and (d) pore size distribution (blue line represents PVDF and red line represents PVDF/EDA/GO).

membrane, the atomic percentages of C and F are 49.7 % and 50.3 %, respectively. However, with the introduction of GO sheets onto the surface of EDA-treated membrane, a new O elemental component was identified, indicating the incorporation of oxygen-containing functional groups from GO onto the membrane surface. This means that GO has effectively alter the PVDF membrane's surface chemistry. This result is aligning with the FTIR analysis (Fig. 5a), where the broad peaks attributed to hydroxyl and carbonyl groups were identified on the membrane surface. In Fig. 8b-ii, the white dots signify the distribution of O elements originating from the GO sheets. The observed O element exhibited uniform distribution across the entire analyzed area, with no indication of significant agglomeration of GO sheets.

Although the CO_2-philic layer does not induce substantial changes in the membrane surface structure, EDA and GO could still diffuse into the membrane pore and anchor to the pore walls, leading to a reduction in pore size. To ascertain whether the coating solution inadvertently penetrated the membrane pores, an analysis of the surface pore size and surface porosity of both the pristine and modified membranes were conducted. As observed in Fig. 8d, there was only a minor decrease in the mean pore size for the PVDF/EDA/GO membrane, indicating comparable pore structures to those of the pristine PVDF membrane, which has a mean pore size of 0.284 ± 0.019 um. Meanwhile, the PVDF/EDA/GO membrane exhibited a tighter pore size distribution, with the average pore size shifting to a lower value of 0.237 ± 0.015 um. These findings suggest that the modification process results in a reduction of pore size, switching the membrane into a slightly "tighter pore" configuration. Both EDA and GO not only adhere to the membrane surface but also attached to the pore walls [30]. Considering that surface pore size significantly influences CO_2 diffusion through the membrane, the reduction in membrane pore size for the modified membrane may lead to notable mass transfer resistance, thereby impacting the movement of CO_2 across the membrane. Therefore, a reduced volume of CO_2 traverses the membrane pores for absorption by the absorbent, resulting in reduced MGA CO_2 absorption performance.

In terms of surface porosity, there was minimal impact, and it remained nearly consistent for both the pristine and modified membranes. The surface porosity of the pristine PVDF membrane is 50.1 ± 1.2 %. Whereas, for the PVDF/EDA/GO membrane, it measures 47.2 ± 2.4 %. Given the preserved surface porosity in the modified membrane, which is nearly aligned to that of the pristine PVDF membrane, it is likely that the intrinsic porous structure of the PVDF membranes remains unaffected. This ensures a similar pathway for CO_2 diffusion through the membranes. The physical properties of the modified membrane (as observed in Figs. 5 and 8) make it challenging to definitively conclude whether they exhibit better CO_2 permeability, owing to the small penetration of EDA and GO into the membrane matrix. The penetration of the coating solutions (EDA and GO) into the pore structure of the modified membrane leads to a slight reduction in pore size, evident in Fig. 8d. This reduction might suggest an anticipated decrease in CO_2 absorption flux, which could counter the intended benefits of the CO_2-philic layer proposed in this work. However, the CO_2-philic layer exists solely as a thin coating attached to the pore walls with a slightly reduced pore size, rather than covering the pores. Therefore, severe pore blockage is avoided. On a positive note, the highly porous structure of the modified membrane remained intact after surface modification (Fig. 8a-ii) and exhibited similar porosity. Maintaining a highly porous membrane structure during the MGA process is of paramount importance, as it ensures minimal mass transfer resistance. This enables the membrane to encounter less resistance by facilitating a rapid CO_2 absorption process and high CO_2 absorption flux.

It is generally known that surface hydrophobicity is a vital element in the MGA process. For the membrane to maintain its non-wetting state through its superhydrophobic characteristics, is essential in ensuring a sustained high CO_2 absorption flux. Therefore, it is crucial to determine whether surface modification via the hydrophilic CO_2-philic layer compromises the membrane wetting resistance (patterned structure) by allowing the coating solution to penetrate the membrane matrix. A comprehensive analysis of membrane hydrophobicity was carried out, with the findings being summarized in Table 1. Before undergoing surface modification, the patterned surface of the PVDF membrane exhibited a WSA of 155.7 ± 2.8° and a WGA of 8.1 ± 0.7°. Whereas the WSA of the opposing non-patterned surface was 85.3 ± 2.3°. After the deposition of CO_2-philic layer on the membrane surface, the WSA decreased to 49.6 ± 2.6°. This shift signifies the transformation of PVDF hydrophobic surface into a hydrophilic surface. This outcome is expected because of the incorporation of hydrophilic functional groups contributed by the CO_2-philic layer (EDA and GO) nested onto the membrane surface. These groups augment the interfacial energy and lead to an increase in membrane surface hydrophilicity [31]. For the patterned surface of the PVDF/EDA/GO membrane, the WSA and WGA of the modified membrane were minimally impacted, measuring 149.7 ± 3.3° and 9.8 ± 1.1°, respectively. The unchanged WSA and WGA values suggest that the penetration of the coating solutions (EDA and GO) did not significantly disrupt the printed hierarchical structure of the membrane, thereby preserving its anti-wetting properties.

In the MGA process, prolonged contact between the membrane surface and the amine absorbent can lead to membrane wetting, causing degradation and compromising the membrane's long-term stability [32]. This deterioration reduces CO_2 mass transfer across the membrane, resulting in a decline in overall CO_2 absorption flux. To assess the membrane's resistance to long-term wetting, the printed patterned surface was exposed to the AMP absorbent for 20 days. The surface pore size and wettability were analysed before and after exposure. Changes were observed after 20 days, particularly in the WSA and WGA. The WSA slightly decreased from 155.7 ± 2.8° to 146.9 ± 3.67°, and the WGA increased modestly from 8.1 ± 0.7° to 28.5 ± 3.67°. These minimal changes are attributed to the hierarchical structure of the printed membrane, which effectively traps air within the rough structure. The trapped air promotes liquid film rupture, thereby preventing the AMP absorbent from penetrating the membrane pores [33]. As a result, the patterned surface remained intact after 20 days of AMP exposure, and successful retaining its anti-wetting ability, as shown in Fig. 9. Similarly, the pore size of the patterned surface showed negligible variation, remaining nearly unchanged from 1.05 ± 0.14 to 1.08 ± 0.09 um after exposure. This consistency aligns with the WSA and WGA results, confirming that only minimal absorbent penetration occurred, and the pore structure was not significantly altered. These findings demonstrate that after 20 days of continuous contact with the AMP absorbent, the membrane's patterned surface effectively inhibited absorbent penetration, preventing wetting and preserving the membrane's performance.

MGA performance

The mixed gas MGA experiments were carried out to assess the potential outcome of the developed membranes, focusing on factors such as membrane surface morphology (surface pore size and porosity), membrane wettability (at the patterned surface) and functional group density (with GO layer). With the consistent wetting resistance of the PVDF/EDA/GO membrane (patterned surface) post-modification, the influence of membrane wetting on MGA performance is negligible. Thus, attention is directed towards assessing the impact of the CO_2-philic layer. Fig. 10a illustrates the CO_2/N_2 separation performances of the composite membrane. Both the modified and unmodified membranes exhibit comparable CO_2 absorption flux. The PVDF/EDA/GO membrane shows a flux of 4.0 x 10^{-3} mol/m^2s, slightly lower than the pristine PVDF membrane at 4.5 x 10^{-3} mol/m^2s. This minor decrease could be attributed to the thin GO layer reducing pore size (~15 % reduction from 0.284 um) and increasing mass transfer resistance, thereby impeding CO_2 diffusion. The incorporation of GO sheets partially covers surface pores, thereby reducing the gas flow pathway and CO_2 diffusion. Although polar functional groups were expected to attract CO_2, promoting closer interaction with the membrane surface to enhance CO_2 absorption, their interaction with CO_2 is insufficient to overcome the mass transfer resistance effectively. Consequently, CO_2 diffusion experiences a slight delay, resulting in a marginal reduction in MGA performance.

Interestingly, the inclusion of the CO_2-philic layer has brought a significant enhancement in CO_2/N_2 selectivity for the PVDF/EDA/GO membrane. Its selectivity is twice as high as that of the pristine PVDF membrane, increasing from 3.0 to 6.0. This notable improvement in CO_2/N_2 selectivity, despite a minor reduction in CO_2 absorption, shed light on the positive impact of the CO_2-philic layer on the overall MGA performance. The presence of GO sheets introduced certain drawbacks. These include the reduction in pore size and alteration of the membrane's tortuosity, which hinders CO_2 diffusion. However, the abundant oxygen functional groups present in GO play a pivotal role in selectively attracting CO_2 molecules. These groups guide the flow of CO_2 towards the amine absorbent for absorption, as shown in Fig. 10b-ii. Given the elevated tortuosity of the membrane, it serves as a major obstacle for the passage of N_2 molecules, thereby contributing to improve CO_2/N_2 selectivity. Notably, the integrated CO_2-philic layer continues to interact with the polar CO_2 molecules from the mixed gas (CO_2/N_2). Although a small fraction of the membrane pores may be covered by the CO_2-philic layer (Fig. 8d) and possibly introducing mass transfer resistance, the results in Fig. 10a showcase a positive achievement, manifesting in enhanced CO_2/N_2 selectivity and maintaining a high CO_2 absorption flux. Similar findings have been reported by Rosli et al. [7,34], highlighting two key factors that contribute to the observed increase in CO_2/N_2 selectivity. First, the polar interaction between CO_2 gas and the oxygen functional groups enhances selective CO_2 transport. Second, the reduced pores size in the membrane increases tortuosity, which impedes N_2 diffusion. Although the increased tortuosity may slightly decrease CO_2 absorption flux, Rosli et al. [34] demonstrated its significant role in improving CO_2/N_2 selectivity. Moreover, owing to the relatively unaffected surface porosity, the pathways for CO_2 transport remain consistent, thereby preventing a significant drop in CO_2 diffusion.

The observed increase in CO_2/N_2 selectivity highlights the fact that the GO-induced CO_2-philic layer interacts with polar CO_2 molecules, facilitating the diffusion of more CO_2 molecules through the membrane. This leads to higher selectivity for CO_2 towards the amine absorbent. Therefore, CO_2 molecules are attracted not only by the amine absorbents, but also by the CO_2-philic functional groups introduced onto the membrane surface (Fig. 10b-ii), further enhancing CO_2/N_2 selectivity. This implies that when the membrane surface contains CO_2-philic functional groups, a minor reduction in surface pore size can be neglected. However, for membrane lacking CO_2-philic functional groups, such as the hydrophobic pristine PVDF membrane, the microporous factor provides easy diffusion pathways for CO_2 gas molecules. Without a CO_2-philic layer, the attractive force for CO_2 depends solely on the affinity of amine absorbent (Fig. 10b-i), leading to low CO_2/N_2

Table 1
Pore size, surface porosity and contact angle of membranes.

Membranes	CO_2-philic surface			Patterned surface	
	Mean pore size (um)	Surface porosity (%)	WSA (°)	WSA (°)	WGA (°)
PVDF	0.284 ± 0.019	50.1 ± 1.2	85.3 ± 2.3	155.7 ± 2.8	8.1 ± 0.7
PVDF/EDA/GO	0.237 ± 0.015	47.2 ± 2.4	49.6 ± 2.6	149.7 ± 3.3	9.8 ± 1.1

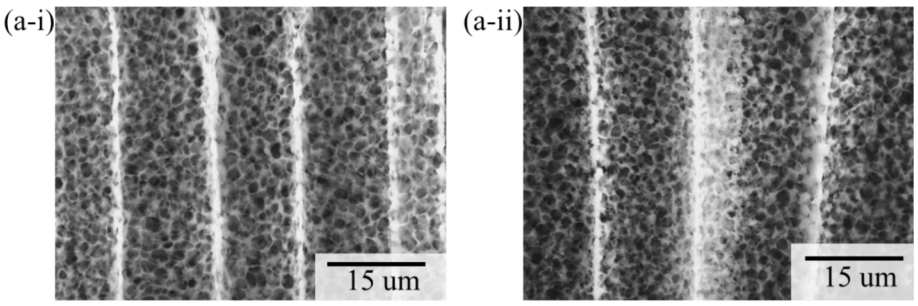

Fig. 9. SEM images of patterned surface of pristine PVDF membrane (i) before and (ii) after 20 days contact with AMP absorbent.

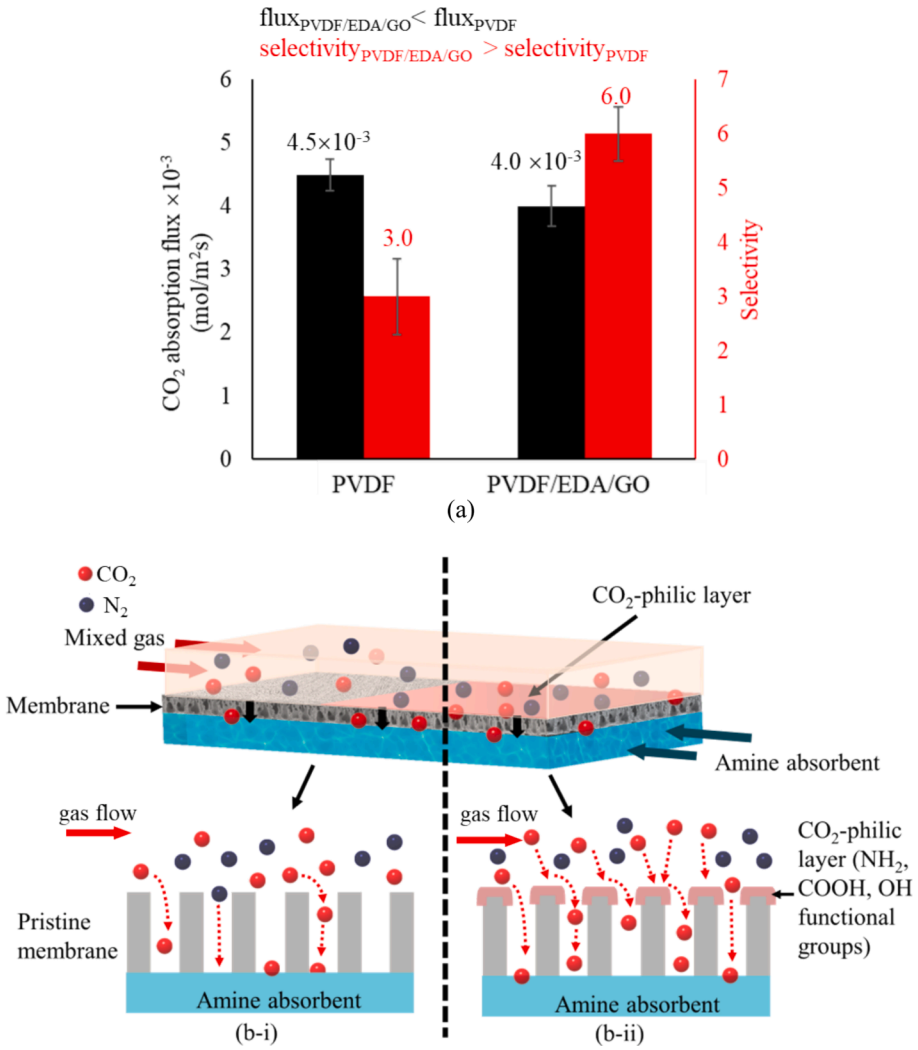

Fig. 10. (a) MGA performance using AMP absorbent and (b) schematic depiction of CO_2 diffusion in MGA (i) without and (ii) with CO_2-philic layers.

selectivity. Thus, even though the pristine PVDF membrane exhibits slightly higher CO_2 absorption flux, the absence of CO_2-philic functional layers contributes to a low CO_2/N_2 selectivity of 3.0. In industrial applications, high selectivity is often prioritized over maximizing CO_2 absorption flux [34]. This low CO_2/N_2 selectivity of pristine PVDF membrane in MGA separation reduces the practicability of membrane separation for purifying CO_2 from mixed gases. Considering this, the pristine membrane falls short of being ideal for MGA applications.

Fig. 11 shows the MGA performance of PVDF/EDA/GO membrane over time for two different CO_2 concentration (20 % CO_2 and 30 % CO_2). The result indicates that the increase in CO_2 absorption flux is apparent as the CO_2 concentration in the gas phase rose. As the concentration increased from 20 to 30 %, the CO_2 absorption flux increased from 4.00 $\times$ 10^{-3} to 5.23 $\times$ 10^{-3} mol/m^{2}s. This phenomenon can be because of an increase in concentration driving force, which consequently enhanced the CO_2 mass transfer rate. Therefore, more CO_2 gas was being absorbed from the mixed gas leading to high CO_2 absorption efficiency. Furthermore, in the MGA process, the chemical reactions between CO_2 and the amine absorbent cause the CO_2 the partial pressure on the permeate side to nearly reach zero when using fresh amine absorbent. This was to ensure that there was a continuous driving force for the transport of CO_2 from the gas side to the liquid side and maintain a constant CO_2

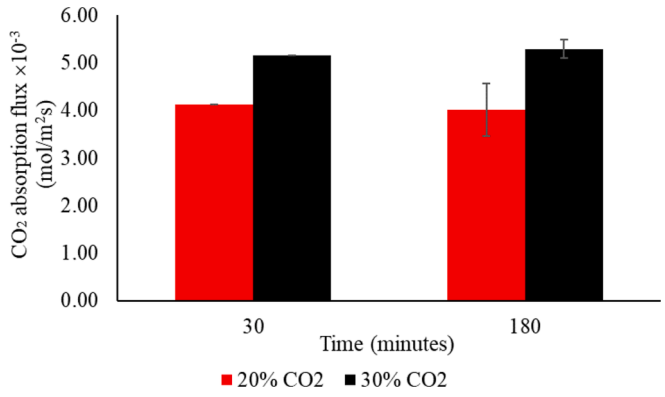

Fig. 11. MGA performance on effect of feed gas concentration.

absorption flux. Hence, the result in Fig. 11 indicated that the PVDF/EDA/GO membrane can be effectively used in CO_2 capture in MGA even dealing with low CO_2 concentration.

There have been several studies focusing on various membranes utilized in the CO_2 capture through MGA process, and their results are compared with the findings of this study, as shown in Table 2. It is recognized that, aside from membrane properties, the CO_2 absorption flux is influenced by operational factors such as the CO_2 concentration and flowrate in the gas phase and absorbent type, concentration and flowrate in the liquid phase. For example, increasing the absorbent concentration results in a more effective rise in CO_2 absorption flux compared to adjustments in feed gas and absorbent flowrate [35]. However, augmenting the amine absorbent concentration not only escalates operational cost, but also raises the potential hazards of handling highly concentrated corrosive amine absorbents during MGA processes. In comparison to existing literature, the amine absorbent used in this work was six-times lower that those reported in literature. Despite this significantly lower amine concentration, the PVDF/EDA/GO membrane developed in this work exhibited markedly higher CO_2 absorption flux, being at least two-times higher than the values reported in the literature. The membrane also demonstrated excellent wetting resistance, as indicated by the high WSA and low WGA compared to values reported in the literature, suggesting minimal penetration of the amine absorbent into the membrane pores. This further supports the suitability of PVDF/EDA/GO membrane for MGA applications. In fact, there is a limited number of reports on gas separation selectivity in the literature, as selectivity is primary determined by the liquid absorbent rather than membrane itself [36]. Consequently, almost all the studies have focused on the CO_2 absorption flux, which does not effectively illustrate the practical viability of MGA in gas purification. The PVDF/EDA/GO membrane developed in this work, which exhibited a reported CO_2 selectivity six-times greater than that of N_2, not only showcased enhanced CO_2 absorption flux but also highlighted its practicability in MGA processes.

The findings of this study highlight the superior performance and practicality of the PVDF/EDA/GO membrane for MGA applications, although some limitations should be acknowledged. This work includes a 20-days stability test, which is considered a relatively long duration compared to other studies in the literature. However, future research should explore the long-term stability of the membrane under varying operational conditions, such as exposure to high pressures and various amines, to ensure its broader applicability in real-world MGA scenarios.

Conclusion

The development of asymmetric wetting membrane holds promise for enhancing CO_2 capture efficiency in MGA operations. By introducing CO_2-philic functional groups onto the hydrophobic PVDF membrane, this work aimed to improve CO_2 affinity and facilitate its absorption during the process. Through the deposition of thin GO layers on PVDF using EDA as a cross-linking agent, this study successfully achieved this enhancement. The resulting PVDF/EDA/GO membrane, enriched with oxygenate functional groups, exhibited a high CO_2 absorption rate of 0.0040 mol/m^{2}s and a CO_2/N_2 selectivity of 6.0. These results clearly indicate the efficacy of the PVDF/EDA/GO membrane in separating CO_2 and N_2 gases in MGA processes, presenting a promising avenue for advancing CO_2 capture technologies.

Table 2
MGA performances from this work and previous literature.

Thin film membrane	WSA &WGA (°)	Input gas	Absorbent parameters	Flux (mol/m^{2}s)	Ref
PVDF + 5 % PTFE	WCA: 92.0 WGA: n/a	CO_2/N_2 (19 vol% CO_2) at 100 mL/min	1 M DEA (50 mL/min)	0.0020	[36]
PVDF-TDMS-1.5	WCA: 150.0 WGA: n/a	CO_2/N_2 (19 vol% CO_2) at 20 mL/min	1 M DEA (50 mL/min)	0.0022	[37]
PDMS/PVDF	WCA: 150.0 WGA: n/a	CO_2/N_2 (9 vol% CO_2) at 200 mL/min	AMP/PZ (100 mL/min)	0.0015	[38]
Dual-layer PVDF-4 % SiO_2-80 %	WCA: 147.2 WGA: n/a	CO_2/N_2 (19 vol% CO_2) at 100 mL/min	1 M DEA (50 mL/min)	0.0031	[39]
PVDF + 8 %PA	WCA: 78.6 WGA: n/a	CO_2/N_2 (19 vol% CO_2) at 130 mL/min	Distilled water (70 mL/min)	0.0013	[40]
PVDF/EDA/GO	WCA: 149.7 WGA: 9.8	CO_2/N_2 (20 vol% CO_2) at 200 mL/min	0.15 M AMP (120 mL/min)	0.0040	This work

CRediT authorship contribution statement

Pei Thing Chang: Writing – original draft, Formal analysis, Data curation. **Qi Hwa Ng:** Supervision. **Pei Ching Oh:** Supervision. **Siew Chun Low:** Writing – review & editing, Supervision, Resources, Conceptualization.

Declaration of competing interest

The authors declare that they have no known competing financial interests or personal relationships that could have appeared to influence the work reported in this paper.

Acknowledgments

The authors express their gratitude for the monetary assistance provided by the Fundamental Research Grant Scheme (FRGS), Ministry of Higher Education Malaysia, with project code FRGS/1/2021/TK0/USM/02/8.

References

[1] S.F. Gargari, S.M. Mirfendereski, J. Ind. Eng. Chem. 128 (2023) 356–368, https://doi.org/10.1016/j.jiec.2023.07.070.
[2] E.L.H. Ng, K.K. Lau, W.J. Lau, F. Ahmad, J. Ind. Eng. Chem. 104 (2021) 231–257, https://doi.org/10.1016/j.jiec.2021.08.028.
[3] A.T. Nakhjiri, A. Heydarinasab, J. Ind. Eng. Chem. 78 (2019) 106–115, https://doi.org/10.1016/j.jiec.2019.06.031.
[4] P.T. Chang, S. Paranthaman, A. Rosli, S.C. Low, ASEAN Eng. J. 12 (1) (2022) 157–164, https://doi.org/10.11113/aej.v12.17336.
[5] P.T. Chang, Q.H. Ng, A.L. Ahmad, S.C. Low, Chem. Eng. Commun. 209 (11) (2022) 1553–1569, https://doi.org/10.1080/00986445.2021.1977926.
[6] P. Jin, C. Huang, J. Li, Y. Shen, L. Wang, R. Soc, Open Sci. 4 (11) (2017) 171321, https://doi.org/10.1098/rsos.171321.

[7] A. Rosli, A.L. Ahmad, S.C. Low, J. Chem. Technol. Biotechnol. 95 (4) (2020) 1073–1084, https://doi.org/10.1002/jctb.6289.
[8] G.H. Teoh, J.Y. Chin, B.S. Ooi, Z.A. Jawad, H.T.L. Leow, S.C. Low, J. Water Process Eng. 37 (2020) 101528, https://doi.org/10.1016/j.jwpe.2020.101528.
[9] F. Zhao, Z. Ma, K. Xiao, C. Xiang, H. Wang, X. Huang, S. Liang, Desalination 443 (2018) 228–236, https://doi.org/10.1016/j.desal.2018.06.003.
[10] Y. Lin, Y. Xu, C.H. Loh, R. Wang, Appl. Surf. Sci. 436 (2018) 670–681, https://doi.org/10.1016/j.apsusc.2017.11.263.
[11] P.T. Chang, Q.H. Ng, A.L. Ahmad, P.C. Oh, S.C. Low, Mater. Today: Proc. (2022), https://doi.org/10.1016/j.matpr.2022.12.082.
[12] Y. Chen, K.-J. Lu, W. Gai, T.-S. Chung, Environ. Sci. Technol. 55 (11) (2021) 7654–7664, https://doi.org/10.1021/acs.est.1c01269.
[13] S. Janakiram, J.L. Martín Espejo, X. Yu, L. Ansaloni, L. Deng, J. Membr. Sci. 616 (2020) 118626, https://doi.org/10.1016/j.memsci.2020.118626.
[14] A. Raza, S. Farrukh, A. Hussain, I.U. Khan, T. Noor, M.H.D. Othman, M.F. Yousaf, Int. J. Energy Res. 44 (10) (2020) 7989–7999, https://doi.org/10.1002/er.5448.
[15] Z. Yarighaleh, O. Bakhtiari, Gas Sci. Eng. 116 (2023) 205049, https://doi.org/10.1016/j.jgsce.2023.205049.
[16] Z. Xu, X. Yan, Z. Du, J. Li, F. Cheng, Sep. Purif. Technol. 251 (2020) 117304, https://doi.org/10.1016/j.seppur.2020.117304.
[17] N. Meng, W. Zhao, E. Shamsaei, G. Wang, X. Zeng, X. Lin, T. Xu, H. Wang, X. Zhang, J. Membr. Sci. 548 (2018) 363–371, https://doi.org/10.1016/j.memsci.2017.11.044.
[18] J. Shen, G. Liu, K. Huang, W. Jin, K.-R. Lee, N. Xu, Angew. Chem. 127 (2) (2015) 588–592, https://doi.org/10.1002/ange.201409563.
[19] P.T. Chang, I.M. Baharuddin, Q.H. Ng, G.H. Teoh, A.L. Ahmad, S.C. Low, Int. J. Energy Res. 46 (4) (2022) 5067–5082, https://doi.org/10.1002/er.7500.
[20] Q. Zhang, Z. Ning, X. Li, X. Ning, F. Wu, J. Zhou, RSC Adv. 13 (48) (2023) 33644–33653, https://doi.org/10.1039/D3RA06767J.
[21] G.H. Teoh, B.S. Ooi, Z.A. Jawad, S.C. Low, J. Environ. Chem. Eng. 9 (4) (2021) 105418, https://doi.org/10.1016/j.jece.2021.105418.
[22] S.A. Hashemifard, A.F. Ismail, T. Matsuura, M.R. DashtArzhandi, RSC Adv. 5 (60) (2015) 48442–48455, https://doi.org/10.1039/C5RA00085H.
[23] F. Cao, H. Gao, H. Ling, Y. Huang, Z. Liang, J. Membr. Sci. 593 (2020) 117439, https://doi.org/10.1016/j.memsci.2019.117439.
[24] Md. Shamim Sheikh, Md. Mahmudur Rahman, Md. Safiur Rahman, K. Yildirim, Mohd. Maniruzzaman, J. Ind. Eng. Chem. 128 (2023) 196–208. Doi: 10.1016/j.jiec.2023.07.048.
[25] Z. Rezaee, T. Mohammadi, O. Bakhtiari, J. Ind. Eng. Chem. 126 (2023) 145–159, https://doi.org/10.1016/j.jiec.2023.06.005.
[26] A. Rosli, S.A. Stephen Paul, S.C. Low, Int. J. Energy Res 45(10) (2021) 15372–88. Doi: 10.1002/er.6810.
[27] K. Eum, D.W. Kim, Y. Choi, X. Duan, M.A. Hillmyer, M. Tsapatsis, A.C.S. Appl, Polym. Mater. 2 (9) (2020) 3859–3866, https://doi.org/10.1021/acsapm.0c00558.
[28] E. te Brinke, I. Achterhuis, D.M. Reurink, J. de Grooth, W.M. de Vos, A.C.S. Appl, Polym. Mater. 2 (2) (2020) 715–724, https://doi.org/10.1021/acsapm.9b01038.
[29] M. Li, Z. Zhu, M. Zhou, X. Jie, L. Wang, G. Kang, Y. Cao, J. Membr. Sci. 627 (2021) 119232, https://doi.org/10.1016/j.memsci.2021.119232.
[30] M.M. Aljumaily, H.M. Alayan, A.A. Mohammed, M.A. Alsaadi, Q.F. Alsalhy, A. Figoli, A. Criscuoli, Appl. Water Sci. 12 (3) (2022) 28, https://doi.org/10.1007/s13201-021-01564-5.
[31] F. Li, L. Chen, Y. Wei, Z. Yin, K. Que, J. Ind. Eng. Chem. 123 (2023) 62–71, https://doi.org/10.1016/j.jiec.2023.03.022.
[32] H. Lim, K. Kim, H.S. Park, J.H. Kang, J. Park, H. Song, J. Ind. Eng. Chem. 122 (2023) 200–209, https://doi.org/10.1016/j.jiec.2023.02.021.
[33] A. Gopikumar, P. Gayathry, A. Vincent, J. Nambikkattu, N.J. Kaleekkal, J. Ind. Eng. Chem. 135 (2024) 493–504, https://doi.org/10.1016/j.jiec.2024.01.060.
[34] A. Rosli, A.L. Ahmad, S.C. Low, Sep. Purif. Technol. 251 (2020) 117429, https://doi.org/10.1016/j.seppur.2020.117429.
[35] H. Rashidi, S. Sahraie, Energy 221 (2021) 119799, https://doi.org/10.1016/j.energy.2021.119799.
[36] M. Du, H. Gong, H. Pang, Q. Shen, Z. Chen, J. Appl. Polym. Sci. 136 (28) (2019) 47767, https://doi.org/10.1002/app.47767.
[37] H. Pang, Z. Chen, H. Gong, M. Du, J. Membr. Sci. 595 (2020) 117536, https://doi.org/10.1016/j.memsci.2019.117536.
[38] Y.-F. Lin, Q. Ye, S.-H. Hsu, T.-W. Chung, Chem. Eng. J. 284 (2016) 888–895, https://doi.org/10.1016/j.cej.2015.09.063.
[39] Z. Chen, Q. Shen, H. Gong, M. Du, Sep. Purif. Technol. 248 (2020) 117045, https://doi.org/10.1016/j.seppur.2020.117045.
[40] H. Pang, H. Gong, M. Du, Q. Shen, Z. Chen, Sep. Purif. Technol. 191 (2018) 38–47, https://doi.org/10.1016/j.seppur.2017.09.012.